



Microstructure of conventional/PBF-LB/M 316L stainless steel hybrid joints brazed with nickel-based brazing alloys

W. Tillmann¹ · J. Bültena¹ · L. Wojarski¹ · A. Crasmöller¹

Received: 2 August 2023 / Accepted: 28 November 2023 / Published online: 13 December 2023
© The Author(s) 2023

Abstract

Due to the additive manufacturing principle, laser-melted materials (PBF-LB/M) such as the austenitic chromium-nickel steel 316L have a different microstructure compared to materials produced by conventional continuous casting. The PBF-LB/M-produced 316L has a thermally metastable, anisotropic microstructure with epitaxially grown grains in which a cellular substructure is located. When brazing hybrid joints from the conventional and additive manufacturing routes with nickel-based brazing alloys, different diffusion mechanisms occur simultaneously in both joining partners. This occurs due to the different microstructural characteristics of the parent materials. The altered diffusion mechanisms lead to a new distinct microstructure in the joining zone, which influences the achievable quality of the brazed joint in a previously unknown way.

Keywords Brazing · Additive manufacturing · PBF-LB/M · Hybrid joints · Stainless steel · Nickel-based brazing alloy

1 Introduction

Powder bed fusion of metal with laser beam (PBF-LB/M) is a powder bed-based additive manufacturing process that is currently the most commonly used in the industry of additive metal manufacturing [1]. Gas-atomized, spherical powders of metals or metal alloys are used as the raw material. The powder is melted (welded) using a laser beam as an energy source and builds up layer by layer to form a structural component [2]. The advantages of the manufacturing principle lie primarily in the high surface quality (Ra, 2 to 17 µm [3]) of the manufactured components compared to other additive manufacturing processes, coupled with high dimensional accuracy (0.24 mm [4]) and the ability to create complex structures with free-form surfaces and internal cavities [5].

Currently, there are economic and technical challenges in laser beam melting, which hinder a more extensive industrial application. The production-related low layer thicknesses and laser scanning speed lead to long building times

resulting in high component costs [5]. The limitation of the maximum component size that can be produced is technically relevant. It is limited, for instance, by the building chamber of the PBF-LB/M machine [6, 7]. As a result of further technical developments, it can be assumed that the building volumes of PBF-LB/M machines will increase in the near future [6]. However, due to the physical principle of PBF-LB/M, it is still not possible to print as large components as by casting. The reasons for this are process-related, thermally-induced, residual stresses in the additive components [8, 9], which arise due to high temperature gradients. These temperature gradients result from the locally high energy input of the laser beam on the surface and the slower heat conduction through the additive component [8, 9]. The amount of induced residual stresses depends on the material used and the size and/or geometry of the component to be processed. If the residual stresses exceed the high-temperature strength of a material, cracking and delamination occur in the additive component during the manufacturing process. By adjusting the process parameters such as the laser power or by preheating the build plate, the temperature gradients and the residual stresses can be reduced but never entirely eliminated [9]. For this reason, a stress-reducing heat treatment is usually performed after part production as a part of the conventional additive process chain [1]. Given the high component cost and the limitations regarding the maximum manufacturable component size, the fabrication of large

Recommended for publication by Commission XVII - Brazing, Soldering and Diffusion Bonding

✉ J. Bültena
julia.bueltena@tu-dortmund.de

¹ Institute of Materials Engineering, TU Dortmund University, Dortmund, Germany

additive components using laser beam melting is difficult [5]. One approach to overcome these restrictions is the production of hybrid components, which exploit the synergies between additive and conventional manufacturing routes. In this case, geometrically simple and/or large-volume parts are manufactured using the less expensive conventional manufacturing route. Complex structures, which cannot be produced at all or only at great expense using conventional manufacturing processes, are produced by using laser beam melting. The additively and conventionally manufactured parts can be joined as a hybrid component by using joining technologies. For this purpose, the brazing technology offers a high potential, since heat treatments can be integrated in the brazing cycle without any additional process steps [10]. Depending on the material and the requirements of the hybrid component, a skillful choice of brazing material offers the opportunity to carry out stress-reducing heat treatments simultaneously during brazing, so that the overall production time of the hybrid component is shortened. Stainless steels such as 316L are often brazed with nickel-based brazing alloys in the temperature range between 970 and 1190 °C [11, 12]. This brazing temperature range overlaps with the solution annealing temperature range of this steel grade (1020 to 1120 °C) [13].

For brazing technology, simultaneous brazing and heat treatment means that the additive material is brazed together with the conventional cast material in the as-built state. However, due to the manufacturing process, the additive and conventional base materials have different microstructure, even though they have the same chemical composition. In contrast to the cast material, the PBF-LB/M microstructure is anisotropic due to the layered material structure. It is characterized by the occurrence of metastable phases, supersaturated solid solutions, and a fine solidification structure as a result of the rapid cooling rate of the PBF-LB/M manufacturing process [14]. Perpendicular to the buildup direction of the additive component, a heterogeneous microstructure with elongated, overlapping melt traces appears which reflects the laser exposure strategy used in the manufacturing process [5]. Along the building direction, the layered material structure becomes visible as periodically occurring and also overlapping semicircular structures [5]. In the case of austenitic stainless steels such as 316L, epitaxial micrograins grow over several melt paths and tracks [15]. Inside these micrograins, a 0.3- [16] to 5- μm hexagonal cellular sub-structure exists, whose formation mechanism has not yet been fully understood [17, 18]. In addition, there are nanoscaled oxide inclusions [17, 19]. These nanoscaled inclusions can be formed by impurities or the oxidation of the metal powder as a result of improper storage or due to the residual oxygen content in the building chamber of the PBF-LB/M machine [20]. Those oxide inclusions are problematic, since the metallic brazing alloy does not wet the

oxide inclusions due to their ionic bonding type. In furnace brazing under high vacuum, no negative influence of oxide inclusions on the brazing suitability of the PBF-LB/M base material can be assumed due to the oxide-reducing effect of the high vacuum [10]. In contrast, the small grain size of the cellular substructure leads to a larger number of grain boundaries compared to the conventionally cast material. Since the diffusion of brazing constituents occurs mainly along grain boundaries [21], more diffusion paths are available in the laser-melted material. A larger number of diffusion paths in the PBF-LB/M material change the diffusion mechanisms during brazing to a yet unknown extent. Since the diffusion processes, which occur during brazing, influence the formation of the microstructure in the joining zone and thus also the mechanical-technological joining properties [21], the effects of the altered diffusion mechanisms on the brazing behavior of PBF-LB/M materials are also unknown. Existing studies on this topic have already demonstrated a completely different microstructure in the joining zone of PBF-LB/M-PBF-LB/M brazing joints for various brazing alloys compared to conventional brazing joints [22, 23].

When brazing hybrid joints of similar materials manufactured by laser beam melting and conventional manufacturing routes, the different microstructures of the base materials result in an uneven diffusion behavior of the brazing components into the joint partners. In the literature, brazed hybrid joints have only been investigated in preliminary work [24, 25]. There, the hybrid joints were made from tool steel 1.2709 with gold-base AuNi18 and from austenitic stainless steel 316L with nickel-based B-Ni2. The PBF-LB/M materials were brazed in the as-built condition. Noticeable differences were found especially in the joints of the austenitic stainless steel. Here, a pore seam appeared at the interface between the brazing metal and the additive base material, which proved to be relevant to failure in tensile tests and led to a tensile strength that was about 33% lower than that of conventional joints. Possible reasons for the formation of the pore seam are the influence of oxide inclusions in the PBF-LB/M material structure, the open porosity on the joining surface of the additive material, and the differences in the diffusion rates of the two joining partners, which could have led to the so-called Kirkendall porosity. Whether this porous seam also occurs with other brazing alloys is not yet known.

Due to the porous seam at the interface and the lack of research in the field of brazed hybrid joints, it is unclear whether the simultaneous brazing and heat treatment process offers an economically viable advantage over the conventional additive process route, in which the additive material is heat treated for stress-relieving reasons right after fabrication [5].

The microstructure of the laser-melted austenitic stainless steel 316L is thermally metastable and starts to dissolve above a temperature of 900 °C [26] until it completely

recrystallizes at a temperature of 1200 °C [27]. Therefore, the stress-reducing heat treatment after additive manufacturing can be designed in such a way that the microstructural morphologies between the additive and conventional manufacturing routes converge. This would have to reduce the differences in the diffusion behavior of the base materials and give the joint the properties of a merely conventional joint. This aspect has not yet been considered in the literature regarding brazing technology.

Based on this current state of research, the aim of this investigation is to analyze the microstructure in the joining zone of brazed hybrid joints made from the austenitic stainless steel 316L using conventional and additive manufacturing routes. In contrast to the existing investigations, the hybrid joints are brazed with the nickel-based brazing alloy Ni 660 (B-Ni5a), considering a simultaneous brazing and heat treatment cycle as well as the conventional additive process route (heat treatment and brazing as separate process steps).

Austenitic steels such as 316L are often brazed with nickel-based brazing alloys such as Ni 660 (B-Ni5a) in a vacuum furnace [28, 29]. Vacuum furnace brazing with nickel-based brazing alloys guarantees good corrosion resistance [10, 12] and at the same time high heat resistance [12, 29] of the brazed joint. As a result, such brazed components are used in nuclear reactors, in chemical apparatus engineering, or for jet and rocket engines [10, 12].

The alloy systems of nickel-based brazing alloys include a large number of different alloy systems to which the melting point depressants (MPD) silicon, boron, chromium, and/or phosphorus are added to lower the melting point of the nickel [Pen21]. MPD have the disadvantage that they form brittle intermetallic phases in the joining zone [29]. The amount of intermetallic phases depends on the brazing parameters such as brazing temperature and holding time [29].

2 Experimental

2.1 Base materials

The conventionally casted base material used for the investigations was a solution-annealed round bar with specification

according to DIN EN 10088-3. The diameter of the bar was \varnothing 20 mm. Table 1 shows the chemical composition according to the material certificate and compares it with the chemical composition of the metal powder used in laser beam melting.

The metal powder used to manufacture the additive components had a particle size distribution of $d_{10} = 10 \mu\text{m}$ to $d_{90} = 45 \mu\text{m}$. This is a common size distribution for powder raw materials used in laser beam melting. With the exception of residual oxygen in the metal powder, the powder raw material and the conventionally casted round bar have similar chemical compositions. The residual oxygen content results from the production process of the metal powder, which was produced by means of gas atomization in a nitrogen atmosphere.

The metal powder was processed to additive components in the form of cylindrical blanks by laser beam melting on a SLM 280 HL machine from SLM Solutions Group. The blanks had a diameter of \varnothing 13 mm with a height of 87 mm. The build-up direction was vertical to the build plate. The layer thickness of the individual material layers of the blanks was 30 μm . Process parameters optimized and provided by the equipment manufacturer were used. During the entire manufacturing process, an argon-inert gas atmosphere with a process pressure of 12 mbar and a maximum oxygen content of less than 0.03% were maintained in the build chamber of the manufacturing plant. To minimize thermal residual stresses, the build plate had a heating temperature of 100 °C. Due to the process principle, the additive manufactured blanks are bonded to the build plate, which is why they were sewn off the build plate directly after the manufacturing process.

2.2 Brazing filler metal

The brazing filler metal used was the nickel-based brazing alloy Ni 660 according to DIN EN ISO 17672 (B-Ni5a according to AWS A5.8). The nominal composition is shown in Table 2. It was selected to ensure that the brazing temperature lies in the upper range of the solution annealing temperature of the austenitic stainless steel 316L. The purpose of this was to test the potential of brazing technology to perform a simultaneous brazing and heat treatment cycle with the aim of reducing the overall production time for hybrid

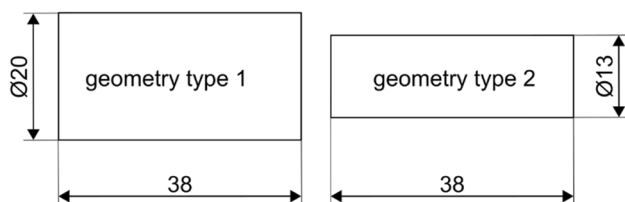
Table 1 Chemical composition of the conventional 316L stainless steel material and the metal powder for the laser beam melting process in weight percentage (values of the material certificates)

Material	Fe	C	Si	Mn	P	S	N	Cr	Ni	Mo	O
Conventional cast 316L (solution annealed)	Bal.	0.021	0.5	1.72	0.044	0.022	0.069	16.65	10.11	2.06	-
PBF-LB/M metal powder	Bal.	0.02	0.69	0.82	0.01	0.01	0.09	17.75	12.6	2.38	0.02

Table 2 Chemical composition of the nickel based-brazing alloy Ni 660 (B-Ni5a) in weight percentage according to DIN EN ISO 17672

Material	Ni	Cr*	Si*	B*
B-Ni5a	72.5	19	7.25	1.25

*Melting point depressants



All measurements in millimeter.

Fig. 1 Semi-finished product geometries

joints made by the additive and conventional manufacturing routes. The brazing material was a foil of 25 μm thickness.

2.3 Semi-finished product geometry

The additively and conventionally produced base materials were processed into the following semi-finished product geometries (see Fig. 1):

- Geometry type 1: \varnothing 20 mm, height 38 mm—conventional semi-finished products only
- Geometry type 2: \varnothing 13 mm, height 38 mm—PBF-LB/M and conventional semi-finished products

To prepare the joining surface for the brazing experiments, one end of each sample was grinded plane-parallel to a surface finish of N6.

2.4 Heat treatment of the PBF-LB/M semi-finished products to consider the conventional additive process route (separate process step prior to brazing process)

After the additive manufacturing process, a stress-relieving solution heat treatment is usually carried out on the 316L [30–32]. This type of heat treatment was also done

within this research with the aim of aligning the PBF-LB/M microstructure to the conventional cast material. The heat treatment was performed in a separate process step prior to brazing in a high vacuum ($<10^{-4}$ mbar) for some—not all—of the laser beam melted semi-finished products with the geometry type 2. For the heat treatment, a vacuum furnace EU 80/1H from IVA Schmetz GmbH was used. The annealing temperature was 1020 $^{\circ}\text{C}$ and was held for 60 min. The temperature control of the furnace batch was in the core of a dummy sample, which had the dimensions of the semi-finished product with geometry type 2 as well. During heating, the heating rate was 10 K/min. To cool the furnace batch, nitrogen gas cooling with a pressure of 4 bar was used. The use of gas cooling allows rapid passing through the sensitization range of the 316L austenitic stainless steel where the material tends to form chromium carbides. The prior to brazing heat-treated samples are called PBFHT.

2.4.1 Analysis of the base materials before the brazing process

All base materials (conventional, PBF-LB/M in the as-built and in the heat-treated condition) were characterized prior to the brazing process. For this purpose, metallographically prepared, longitudinal, and transverse sections were made. To visualize the microstructure, the sections were etched with V2A etchant (hydrochloric acid 37%, nitric acid 65 %). Subsequently, the sections were examined by light microscopy. The light microscopic images were taken with a light microscope BX51M from Olympus K. K at a magnification of $\times 20$. The scanning electron micrographs were only made for the transverse sections—the later joining surface. For this purpose, a JSM 7001F field emission scanning electron microscope from Jeol was used in secondary electron contrast. The images were acquired at $\times 5000$ magnification with an accelerating voltage of 20 kV and an emission current of 75 μA .

2.5 Brazing experiments

Using the different base materials, hybrid and conventional joints were brazed (see Table 3). The brazing tests considered the process routes according to a simultaneous brazing and heat treatment cycle as well as the conventional additive process route (separate brazing and heat

Table 3 Overview of the used base materials and brazed joints

Base material	PBF PBFHT C	As-built Heat treated at 1020 $^{\circ}\text{C}$ for 60 min Conventional material
Vacuum brazed joints	C/PBF C/PBFHT C/C	Hybrid joint with combined brazing and heat treatment process Hybrid joint with separated brazing and heat treatment process Conventional joint

treatment). The conventional part of the hybrid joints always had the shape of the semi-finished product of geometry type 1 with a diameter \varnothing 20 mm. The additive materials exhibited the shape of the semi-finished product geometry type 2 with a diameter \varnothing 13 mm. The joining surface was parallel to the building direction of the semi-finished parts. In each case of the conventional brazed joints, a conventional semi-finished part of type 1 (\varnothing 20 mm) was brazed to a conventional semi-finished part of type 2 (\varnothing 13 mm). For illustrational reasons, from now on, the abbreviation PBF will be used in the diagrams and figures instead of PBF-LB/M. The same applies to the conventional material, where the abbreviation C is used.

2.5.1 Sample preparation—semi-finished parts and the brazing foil

Before the brazing experiments, the semi-finished parts were cleaned in an ultrasonic ethanol bath for 5 min. The brazing foil was roughened with an abrasive fleece to remove the oxide layer and any contamination. Then, it was cut to a diameter of \varnothing 15 mm. The cut-out foil diameter of \varnothing 15 mm is 2 mm larger than the diameter of the joining surface (\varnothing 13 mm). This oversize guarantees a sufficient amount of brazing filler metal to completely fill the installed gap, even in the case of scratches and unevenness on the prepared joining surface. After cutting, the brazing foil was cleaned manually with ethanol to remove impurities.

After the cleaning processes, the semi-finished parts were placed in a brazing fixture, which centers the different types of geometries (\varnothing 20 mm and \varnothing 13 mm) on each other. Then, the brazing foil was applied. For each brazing joint, two foil cuttings were placed double-layered between the semi-finished parts. Thus, the installed gap is set to 50 μ m via the foil thickness ($2 \times 25 \mu$ m), which is a commonly used gap width in the industry. Fig. 2 shows the sample geometry prior to brazing.

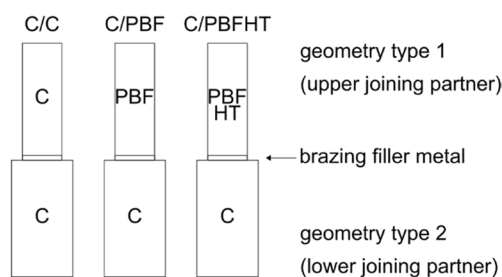


Fig. 2 Sample geometry

2.5.2 Brazing processes

For the brazing tests, a total of two furnace batches were carried out. For each furnace run, hybrid brazed joints were produced according to a combined and a separate brazing and heat treatment cycle, as well as conventional brazed joints. The simultaneous production of the different brazed joints within one furnace batch increases the comparability of the brazed joints with each other. This makes it possible to avoid variations in the results of different brazing processes due to fluctuations, which may also influence the microstructure in the joining zone when the test parameters are the same.

All brazing processes were conducted in a high-temperature vacuum furnace EU 80/1H from IVA Schmetz GmbH in a high vacuum with a pressure of less than 10^{-4} mbar. The control of the furnace batch was based on the temperature measurement in the core of a dummy sample, which had the dimensions of the joint geometry to be brazed. During the heating process, the heating rates were 10 K per min. Also, 15-min dwell stages were performed at 450 °C and 1015 °C. These dwell stages served to achieve a homogeneous temperature distribution within the furnace batch. The brazing temperature was 1190 °C for all brazing cycles.

The holding time was varied between 15 and 60 min in order to analyze the effects of altered diffusion mechanisms occurring in the additive and conventional base materials on the microstructure in the joining zone. Cooling from the brazing temperature to room temperature was performed in the same way as for the heat treatment of the semi-finished parts. Therefore, nitrogen gas cooling with a pressure of 4 bar was used.

To ensure statistical reliability, two brazing joints were brazed per manufacturing route (C/C, C/PBF, C/PBFHT) and holding time (15 min/60 min). Due to the high material costs of the additive semi-finished parts, it was not possible to achieve a higher level of statistical validation. Table 4 shows the experimental matrix.

2.6 Evaluation of the brazing experiments

The evaluation of the brazing experiments included the analysis and the comparison of the microstructures in the joining zone of the hybrid (C/PBF, C/PBFHT) and conventional brazed joints (C/C). The analyzed microstructural characteristics of a joining zone were the brazing gap width, the depth of the diffusion zones (top/bottom), and the number, shape, and type of brittle phases in the brazing gap and the diffusion zones. The microstructural evaluation was performed by scanning electron microscopy and energy dispersive X-ray spectroscopy on metallographically prepared longitudinal sections of the brazed joints. The identical field emission scanning electron microscope with the same measurement

Table 4 Experimental matrix

Manufactured joints	Geometry type		Brazing alloy	Brazing temperature °C	Holding time Min	Number of samples -
	Geometry type 1 Lower joining partner	Geometry type 2 Upper joining partner				
C/PBF	C	PBF	B-Ni5a	1190	15	2
C/PBFHT	C	PBFHT	B-Ni5a	1190	15	2
C/C	C	C	B-Ni5a	1190	15	2
C/PBF	C	PBF	B-Ni5a	1190	60	2
C/PBFHT	C	PBFHT	B-Ni5a	1190	60	2
C/C	C	C	B-Ni5a	1190	60	2

settings as in Section 2.3.2 was used for the investigations. Scanning electron microscope image acquisition was performed at $\times 250$ and $\times 500$ magnification in backscattered electron contrast. On the SEM images at $\times 250$ magnification, the width of the brazing gap and the depths of the diffusion zones of the upper and lower joining partner were measured using the integrated software of the scanning electron microscope. Per sample, all microstructural characteristics (brazing gap width, diffusion zone depth) were measured at three locations and were then arithmetically averaged. For statistical reasons, the microstructure of two brazed joints was analyzed per parameter set. The parameters determined per longitudinal section were also arithmetically averaged.

To determine the chemical composition of the various phases in the joining zone, the X-Act type energy dispersive X-ray spectrometer (EDS) from Oxford Instruments that is integrated into the scanning electron microscope was used. The EDS measurements were obtained at the locations where the SEM images were taken at $250\times$ magnification. The EDS measurements were performed pointwise with a measurement time of 10 s for the different phases (solid solutions, brittle phases) in the joining and diffusion zones. The determination of the chemical composition and the evaluation of the EDS measurements were carried out using the INCA program from Oxford Instruments.

3 Results

3.1 Microstructural morphology of the base materials prior to the brazing process

Fig. 3 compares the microstructures of the base materials conditions prior to brazing by means of optical micrographs in longitudinal and transverse sections. The transverse section represents the subsequent joining surface for the brazing experiments. The conventional material has an isotropic microstructure exhibiting visible twin grain boundaries. Uniformly distributed manganese sulfide inclusions are also

evident in the longitudinal section. The elongated shape of the manganese sulfides results from the cold rolling process of the conventional round bar.

In contrast, the laser-melted material in the as-built state has an anisotropic microstructure. In the longitudinal section, melt paths and melt traces of the additive manufacturing process are visible, as well as the epitaxially grown microstructure of the micrograins. In the transverse section, the micrograins and the exposure strategy of the laser beam used during the PBF-LB/M manufacturing process are revealed. The grain size of the micrograins is smaller in the transverse section than in the longitudinal section. However, in both sections, it is larger than that of the conventional material. No defects such as bonding defects and key-hole pores are visible in the light microscopy images. The used PBF-LB/M manufacturing parameters resulted in a high component density, which was determined to be 99.98%. Scanning electron micrographs of the joining surface on Fig. 4 show the cellular sub-structure within the micrograins, which is already known from the literature. The grain size of this sub-cellular structure is smaller than the grain size of the conventional material. The white precipitates within the cellular substructure are probably the nanoscale oxide inclusions known from the literature.

A solution heat treatment process at $1020\text{ }^{\circ}\text{C}$ for 60 min in a high vacuum led to a change in the PBF-LB/M microstructure. The melt traces and melt paths started to slowly dissolve due to the heat treatment but did not completely disappear. The grain size of the micrograins increased in both transverse and longitudinal sections. Based on the optical microscopy images, no heat treatment-induced change in porosity can be detected. The scanning electron micrographs of the joining surface in Fig. 3c show that the cellular substructure has dissolved due to the heat treatment. Furthermore, micropores can be seen on the images both inside the micrograins and at their grain boundaries. The size of the pores is larger at the grain boundaries than inside a micrograin. Eventually, the pores inside the micrograin are located at the former grain

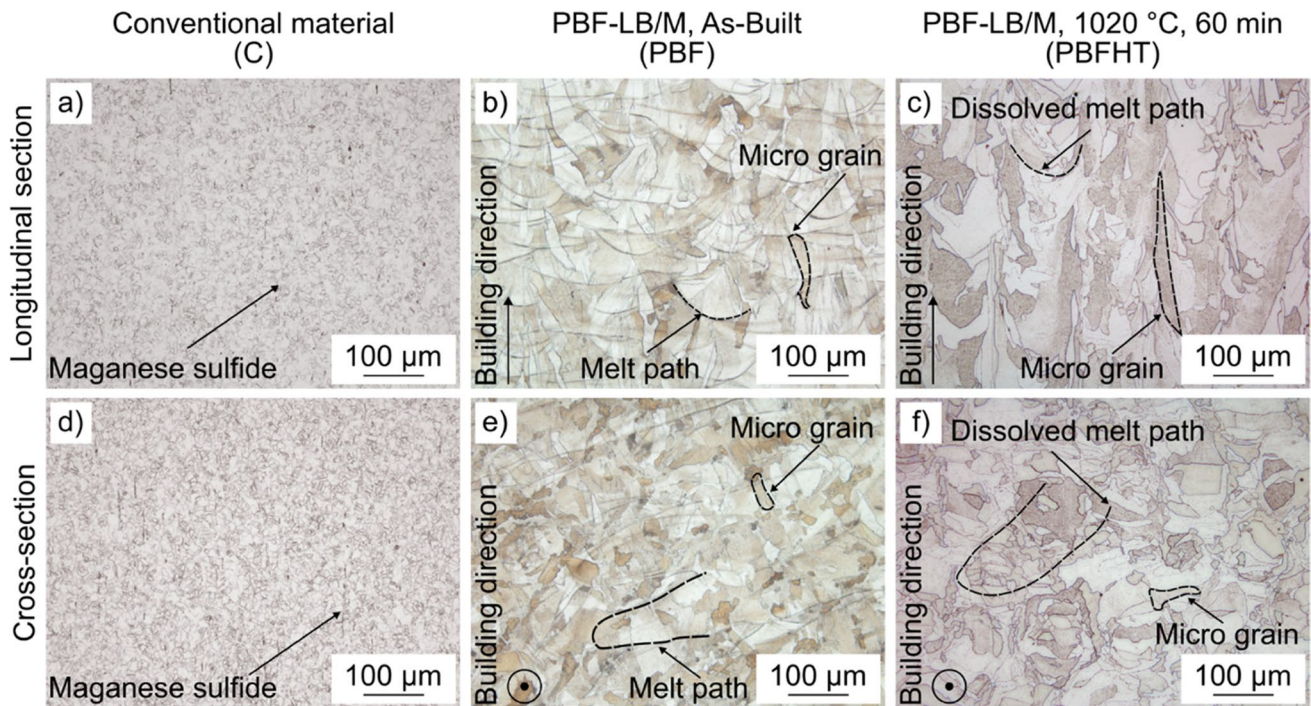


Fig. 3 Comparison of the microstructures between the conventional material and the PBF-LB/M material in the as-built condition and after heat treatment at 1020 °C for 60 min in a high vacuum

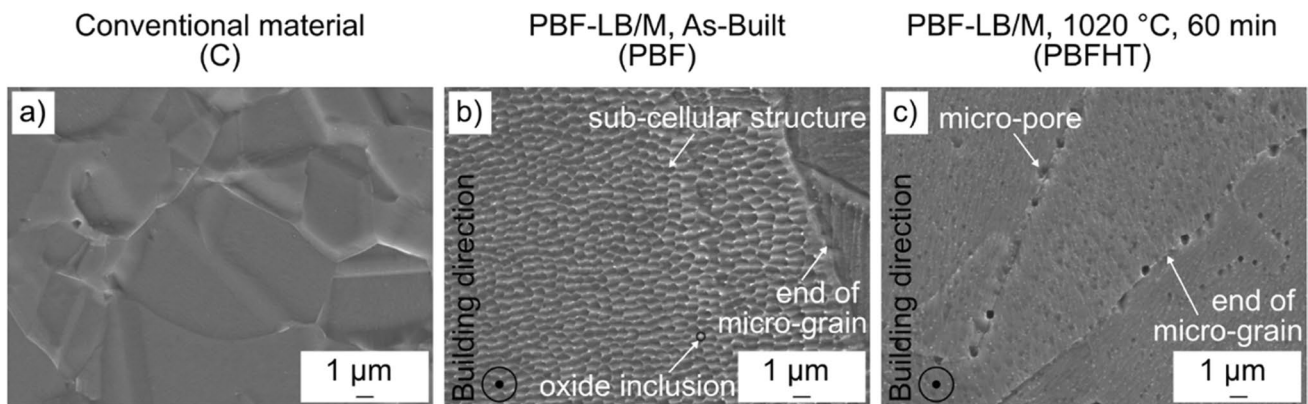


Fig. 4 Scanning electron micrographs of the joining surface of the **a** conventional material and the laser beam melted material in the **b** as-built state and **c** after heat treatment at 1020 °C for 60 min in a high vacuum

boundaries of the cellular sub-structure. The dissolution of the cellular sub-structure as well as the pore formation coincide with the results of Salman's research group [33]. In this context, the research group attributed the pore formation to the heat treatment-induced grain growth including microstructural coarsening. In the solution-annealed condition, no nanoscale oxide inclusions are visible on the joining surface. These were presumably reduced by the high vacuum prevailing during the heat treatment.

3.2 Microstructure in the joining zone

Fig. 5 compares the microstructures of the hybrid composites (C/PBF, C/PBFHT) brazed at 15 and 60 min holding time with those of the conventional reference brazes (C/C) using scanning electron micrographs.

Different microstructural areas in the joining zone can be distinguished from one another within a raster electronic image: In the center of the joining zone, the brazing material

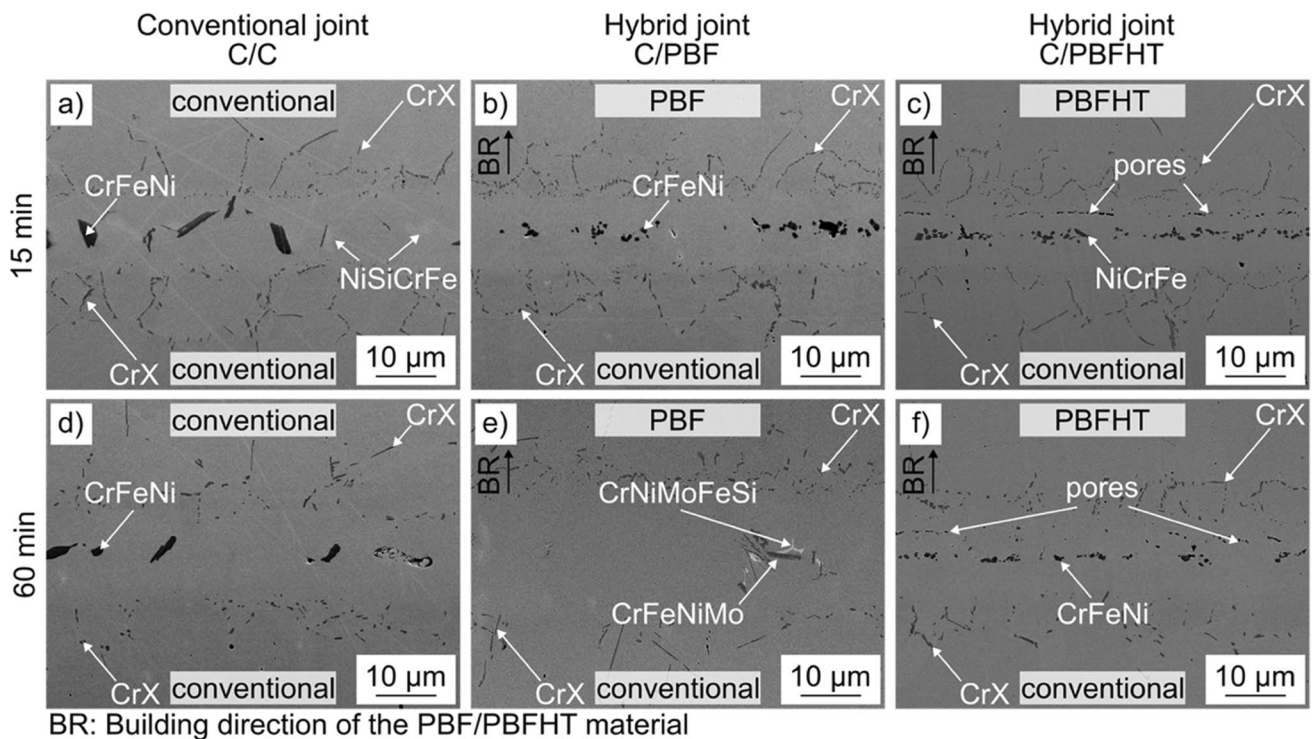


Fig. 5 Microstructure of the various brazed joints as a function of the holding time—intermetallic phases

appears lighter than the base materials, which is due to its chemical composition (upper or lower image area). Within the brazing material, other phases are visible. In brazing technology, these phases are referred to as intermetallic phases. In the case of nickel-based brazing alloys, these precipitates often consist of the MPD of the brazing alloy like silicon, boron, and chromium. In addition, there is a diffusion-affected zone (DAZ) on both sides of the braze. The DAZ can be recognized by dark precipitates at the brazing material/base material interface and at the grain boundaries of the base material. These precipitates also consist of the MPD of the brazing filler metal.

The scanning electron micrographs show that the brazing material has a predominantly light gray, almost homogeneous matrix. This can be seen in all brazed joints (C/C, C/PBF, C/PBFWB). According to the EDS measurements, the matrix of the brazing material consists predominantly of a Ni, Cr, Fe, and Si solid solution. The Fe in the solid solution results from the chemical composition of the base material. Due to the diffusion processes taking place during brazing and due to the dissolution of the base material by the molten brazing filler metal, some of the iron atoms of the base material migrate into the joining zone, thus forming an iron-enriched nickel solid solution with the brazing alloy. Due to the longer diffusion processes, the Fe content in the solid solution increases from holding times of 15 to 60 min. Also, owing to the longer diffusion processes with

increasing holding time, the resulting brazing gap width increases. However, no difference in resulting brazing gap width was observed between the conventional and hybrid brazed joints (C/C, C/PBF, C/PBFHT). The reason for this could be the small number of samples with a statistical confidence level of two.

In addition to the Ni, Cr, Fe, and Si solid solutions, EDS measurements shown in Table 5 indicate areas of comparatively low silicon content in the braze material. On the SEM images, the silicon-rich phases appear slightly brighter than the surrounding Ni, Cr, Fe, and Si solid solutions. More silicon-rich phases are present in all brazed joints but are particularly visible in the SEM images of the conventional joints C/C brazed with a holding time of 15 min

For all brazed joints (C/C, C/PBF, C/PBFHT) with a holding time of 15 min, the intermetallic phases are present in the center of the brazing material. There, they form a continuous brittle phase band. EDS measurements indicate that the chemical composition of the intermetallic phases is primarily Cr, Fe, and Ni. According to the literature, the MPD boron should also be present in these precipitates as a constituent of the Ni 660 alloy [32]. However, due to the small atomic size, this chemical element cannot be detected with the used EDS detector. Moreover, in smaller precipitates, elements of adjacent phases can also be detected due to the size of the EDS measurement spot. Probably, this is

Table 5 Chemical composition of the different phases measured by EDS in weight percent

Joint	Holding time	Phase	Chemical Elements in weight percent					
			Ni	Cr	Si	Fe	Mn	Mo
C/C	15	CrFeNi	5.34	79.77	0.48	11.73	0.96	1.71
		NiSiCrFe	61.95	10.15	16.35	7.59	2.48	1.48
		CrX	5.06	37.73	0.22	51.80	1.73	3.46
	60	CrFeNi	2.43	81.34	0.05	12.69	1.04	2.45
		CrX	3.92	44.46	0.22	45.16	2.03	4.21
		CrFeNi	36.65	39.63	4.50	14.46	0.92	3.85
C/PBF	15	CrX	6.37	41.27	0.66	45.74	1.16	4.80
		CrFeNi	36.65	39.63	4.50	14.46	0.92	3.85
		CrFeNiMo	55.26	12.55	13.79	13.16	1.08	4.17
	60	CrNiFeSiMo	19.95	42.03	7.85	12.29	0.69	17.19
		CrX	2.76	48.80	0.25	41.72	2.11	4.36
		CrFeNi	39.21	39.97	4.45	14.74	0.68	0.94
C/PBFHT	15	NiCrFe	39.21	39.97	4.45	14.74	0.68	0.94
		CrX	8.11	28.22	0.34	58.63	1.99	2.72
	60	CrFeNi	9.30	80.96	0.58	6.96	0.66	1.54
		CrX	2.55	51.32	0.15	40.65	1.56	3.76

the case for both Fe and Ni, which were also measured in the brittle phase band. Based on the results of brazing experiments with the chemically similar brazing filler metal MBF-51 used for brazing 316L by Rabinkin et al. [32], the blocky intermetallic phases are identified as chromium borides.

In addition, all brazed joints with a holding time of 15 min exhibit intermetallic phases with a dark, block-like structure. In the conventional joints (Fig. 3a), the phases are larger and in smaller quantities than in the C/PBF and C/PBFHT hybrid joints. In contrast, the brittle phases in the hybrid joints (Fig. 3b–c) are much finer in structure and exist in greater quantity than in the conventional joints. The different amounts and properties of the brittle phases between the conventional (C/C) and the hybrid joints (C/PBF and C/PBFHT) are probably due to the different diffusion mechanisms and diffusion rates that occur during brazing. These differences result from the different microstructures of the joining partners due to the manufacturing process. Despite the heat treatment performed prior to the brazing process, which resulted in a convergence of the microstructures of PBF-LB/M and conventional materials, no significant difference in chemical composition, shape, and quantity was observed between the brittle phases in the hybrid joints C/PBF and C/PBFHT. Differences in the chemical composition of the intermetallic phases of the hybrid joints might be related to the size of the measuring spot of the EDS analysis. Due to the small size of the intermetallic phases in the hybrid joints, the surrounding nickel solid solution could have been measured as well.

For all joints, an increase of the holding time from 15 to 60 min (Fig. 3d–f) leads to a significantly lower number of brittle phase formation sites. This is due to the longer diffusion processes that take place with increasing holding time. Thereby, the MPD, such as boron, diffuse more intensively

into the base material. Due to the longer diffusion processes, the amount of MPD in the center of the joining zone is lower, which contributes to a significantly reduced brittle phase formation in this area [32].

In the conventional C/C and in the hybrid joint C/PBF with a holding time of 60 min, the brittle phases are more isolated and no longer present as a continuous band (Fig. 3d, e). In contrast, the brittle phases in the C/PBFHT hybrid joint are still evident in the form of a band. However, this phase band is interrupted much more frequently compared to a 15-min holding time (Fig. 3f). It is also noticeable that acicular light gray and white precipitates appear in the C/PBF hybrid joint (Fig. 3e). EDS measurements show a high content of silicon and chromium. Such acicular phases were not observed in the C/PBFHT hybrid joint or in the conventional C/C joint. It is known that Cr_xB_y , Ni_xSi_y , and Mo_xSi_y phases can form during brazing of stainless steel with nickel-based brazing alloys. The formation depends on the temperature, holding time, and chemical composition of the braze [32]. The reason for the different phase formation between the hybrid compound C/PBF and the other brazing compounds is probably the diffusion processes occurring there. For a more precise assessment, further detailed investigations of the diffusion processes occurring during the brazing of hybrid joints are required.

In addition to the phase formation, the C/PBFHT hybrid joint shows an increased pore formation at the brazing material/PBF-LB/M interface. This pore formation is present at a holding time of 15 and 60 min. In contrast, the conventional C/C and the hybrid joints C/PBF are largely free of pores. The pores in the hybrid joints C/PBFHT consist of various individual pores that merge to form larger pores with a semicircular shape. Differences in pore morphology between a holding time of 15 and 60 min were not observed. These

observed semicircular pores show a high similarity to the Kirkendall porosity found by Park et al. in soldered Cu/Sn/Cu microbumps [34]. The reason for the pore formation underlying the Kirkendall effect is different diffusion rates of the brazing/soldering constituents into the materials [34]. At present, it is unclear why this pore formation only occurs while brazing the additive material that has been solution-annealed prior to the brazing process. Future investigations will commence here and seek to establish a suitable theory for the mechanism of pore formation by determining the diffusion velocities of the brazing constituents into the base materials. In this context, the formation of the intermetallic phases of the hybrid joints will also be investigated in more detail.

3.2.1 Microstructure of the diffusion-affected zone

In addition to phase formation and resulting brazing gap width in the joining zone, the diffusion-affected zones of the various brazing joints were analyzed. The DAZ in the scanning electron micrographs is characterized by dark precipitates at the brazing material/base material interface and the grain boundaries of the respective base material. Fig. 6 summarizes the measured diffusion depth of the upper and lower joint partner for the different brazed joints (C/C, C/PBF, C/PBFHT) as a function of the holding time (15 min/60 min).

In general, a longer holding time leads to an increase in the diffusion depth in the respective joining partner due to the longer-lasting diffusion processes. However, the measurement results indicate that the type of upper joining partner (C, PBF, PBFHT) has an influence on the diffusion depth in the lower, conventionally manufactured joining partner (C/C, C/PBF, C/PBFHT). At present, the cause of this is unknown and requires further investigation. In addition, a comparison of the diffusion depths in the conventionally and the additively manufactured base material indicates a tendency towards a lower diffusion depth in the PBF-LB/M material in the upper joining partner. The smaller grain size is seen as a possible cause for the lower diffusion depth in the additive material. As a consequence of the smaller grain size on the additive joining surface, the same number of

MPD depressants must diffuse over a larger grain boundary surface than in the conventionally produced base material.

A more detailed microscopic examination of the diffusion-affected zones of the upper joining partners (C, PBF, PBFHT) for the various brazed joints (C/C, C/PBF, C/PBFHT) reveals further distinguishing features of the hybrid joints (C/PBF, C/PBFHT). Figure 7 shows exemplary SEM images of the DAZ of the upper joining partners for the different joints, using the example of the brazing joints with a holding time of 15 min.

For both conventional and hybrid joints, the diffusion-affected zones can be divided into two areas in which the intermetallic phases show different characteristics. The first

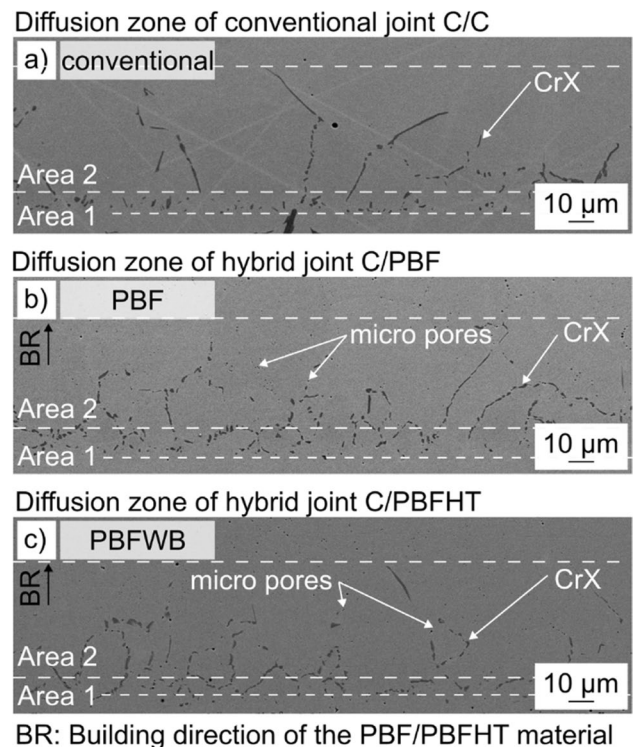
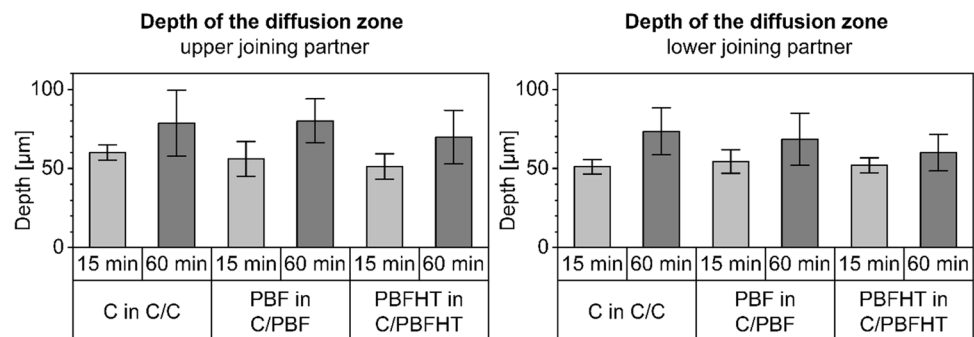


Fig. 7 Intermetallic phases in the joining zone for the hybrid and conventional brazing composites at a brazing temperature of 1190 °C for 15 min

Fig. 6 Depth of the diffusion zone of the upper and lower joining partner



area is located directly at the brazing material/base material interface. Here, the intermetallic phases have a seemingly random arrangement and a smaller shape. The second area is the one directly behind the brazing material/base material interface, where the intermetallic phases precipitate at the grain boundaries of the base material. The precipitates in this area are significantly larger than those precipitated in the area of the brazing material/base material interface. The presence of the different areas of a diffusion-affected zone is consistent with the results of other research [35, 36]. A direct comparison of the hybrid joints to the conventional joints shows that the two areas of the diffusion-affected zones (interface brazing material/base material, base material) cannot be differentiated as clearly in the additively produced joining partners of the hybrid joints as in the conventional joints. In addition, the diffusion zones of the additively produced base materials (PBF, PBFHT) contain more precipitates on a smaller surface area, which means that these precipitates are more concentrated there than in the diffusion zone of the conventional material. There is no discernible difference between the intermetallic phases in the PBF-LB/M base material brazed in the as-built and solution-annealed condition. In general, the size of the precipitates in the diffusion zones of the PBF-LB/M materials is smaller, but their number is larger than in the conventional material. This is consistent with the precipitation characteristics of the intermetallic phases in the joining zone, which also have a larger quantity with a smaller size in the hybrid joints. Since the chemical composition of the additive and the conventional base material is approximately the same, the reason for this is probably the characteristic PBF-LB/M microstructure.

EDS measurements prove an increased chromium content of the intermetallic phases in the diffusion zone for both the conventional (C) and the additive base materials (PBF, PBFHT). This type of intermetallic phases has already been identified as Cr_xB_y in other research on brazing austenitic steels with boron containing nickel-based brazing alloys [37]. Since the chemical element boron is not detectable with the EDS detector used, it can be assumed that the precipitated intermetallic phases in the diffusion zones of the brazing joints of this work are also Cr_xB_y phases. Due to the inability to detect boron, the designation CrX is therefore used in all scanning electron micrographs of this work.

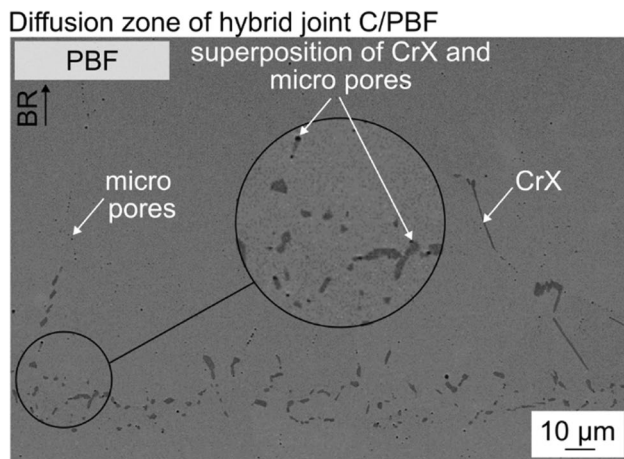
In addition to the different phase formations in the diffusion zones of the PBF-LB/M base materials, a formation of micropores was observed in the PBF-LB/M bulk material after the brazing process. This micropore formation occurs in both the PBF-LB/M material which has been solution-annealed prior to the brazing process (PBFHT) and the PBF-LB/M material brazed in the as-built condition (PBF). These micropores are visible at the grain boundaries of the PBF-LB/M base materials (PBF, PBFHT) as well as inside the

grains. The size of the pores at the grain boundaries is larger than the size of the pores within the grains. The micropores may result from smaller pores in the additive material resulting from the PBF-LB/M manufacturing process, which were too small to be detected by SEM during base material characterization. As a result of the thermal exposure of the brazing process, they possibly diffused mainly along the grain boundaries and then coalesced into larger micropores. The reason for the existence of the micropores inside the grain boundaries is presumably the cellular sub-structure of the additive material present in the as-built state. This cellular sub-structure is thermally metastable and starts to dissolve above a temperature of 900 °C. Due to the brazing temperature of 1190 °C, the cellular sub-structure is no longer present in the PBF-LB/M base materials after the brazing process. It is also possible that there were small pores at the grain boundaries of the cellular substructure, which coalesced into larger pores during the brazing process and remained in the micrograins surrounding the substructure after the dissolution of the cellular structure above 900 °C. A difference in the size of the micropores between the PBF-LB/M base material brazed in the as-built and solution-annealed condition, as well as the influence of an increasing holding time, has not yet been investigated. This study could verify or falsify the ideas about the cause-effect relationships of pore formation. Further investigations are also needed to determine whether the size and concentration of the micropores increases in the region close to the joining zone. This is of significant importance for brazing technology, because an increase in the size and concentration of the micropores in the direction of the interface brazing/base material would be a further sign for the occurrence of Kirkendall porosity.

Figure 8 shows the effects of micropore formation exemplified by a detailed image of the diffusion zone of the PBF-LB/M material as part of a C/PBF hybrid joint brazed at a brazing temperature of 1190 °C and a holding time of 60 min. The micropores overlap with the intermetallic phases precipitated in the diffusion zone. This superposition may represent weak points under mechanical stress, though this could have a negative effect on the joint strength. The impact of this is currently under investigation.

4 Summary and conclusion

Compared to the conventional joints C/C, the additive hybrid joints C/PBF and C/PBFWB have a different microstructure. In all manufactured joints, C/C, C/PBF, and C/PBFHT brittle phases are present. In the conventional joints, the brittle phases in the microstructure are larger and in smaller quantities than in the C/PBF and C/PBFHT hybrid joints. In contrast, the brittle phases in the hybrid joints are much



BR: Building direction of the PBF material

Fig. 8 Superposition of the intermetallic phases and the micropores in the diffusion zone exemplified by the hybrid composite C/PBF brazed at 1190 °C for 60 min

finer in structure and exist in greater quantity than in the conventional joints. In summary, it can be stated that the characteristic PBF-LB/M microstructure has an influence on the formation and quantity of intermetallic phases in both the joining and diffusion-affected zones of brazed hybrid joints. At the same time, the additive material is influenced by the thermal exposure of the brazing process in such a way that micropores are formed. These micropores lead to an overlap with the precipitates in the diffusion zone. The effects of the different phase formation as well as the superposition of the micropores on the mechanical joint strengths are unknown so far.

Solution heat treatment prior to brazing leads to an approximation of the PBF-LB/M microstructure morphology to the conventional cast material. But while brazing, semicircular pores form in the joining zone regardless of a holding time of 15 min or 60 min. The cause of the pore formation is assumed to be the occurrence of the Kirkendall effect as a result of the different diffusion rates of the brazing constituents in the additive and conventional joining partners. The influence of the semicircular pores on the mechanical joint strength will be investigated.

Supplementary Information The online version contains supplementary material available at <https://doi.org/10.1007/s40194-023-01652-x>.

Acknowledgements The research project IGF 21.693 N/“Systematische Untersuchung der parameterabhängigen Mikrostrukturausprägung auf die mechanisch-technologischen Eigenschaften von gelöteten Verbunden aus SLM generierten und konventionell hergestellten Werkstoffen” from the Research Association for steel Application (FOSTA), Düsseldorf, is supported by the Federal Ministry of Economic Affairs and Climate Action of the German Federation of Industrial Research Associations (AiF) as part of the program for promoting industrial cooperative research (IGF) on the basis of a decision

by the German Bundestag. The project is carried out at the Institute of Materials Engineering at the TU Dortmund University.

Funding Open Access funding enabled and organized by Projekt DEAL.

Declarations

Competing interests The authors declare no competing interests.

Open Access This article is licensed under a Creative Commons Attribution 4.0 International License, which permits use, sharing, adaptation, distribution and reproduction in any medium or format, as long as you give appropriate credit to the original author(s) and the source, provide a link to the Creative Commons licence, and indicate if changes were made. The images or other third party material in this article are included in the article’s Creative Commons licence, unless indicated otherwise in a credit line to the material. If material is not included in the article’s Creative Commons licence and your intended use is not permitted by statutory regulation or exceeds the permitted use, you will need to obtain permission directly from the copyright holder. To view a copy of this licence, visit <http://creativecommons.org/licenses/by/4.0/>.

References

1. Celik E (2020) Additive manufacturing: science and technology. De Gruyter graduate. Walter de Gruyter GmbH, Berlin, Boston
2. Munsch M (2013) Reduzierung von Eigenspannungen und Verzug in der laseradditiven Fertigung, Schriftenreihe Lasertechnik, v.6., 1st edn. Cuvillier Verlag, Göttingen
3. Kruth J-P, Vandenbroucke B, van Vaerenbergh J et al (2005) Benchmarking of different SLS/SLM processes as rapid manufacturing techniques. *Laser 1:3D*
4. Özsoy K, Aksoy B, Salman OKM (2021) Investigation of the dimensional accuracy using image processing techniques in powder bed fusion. *Proc Inst Mech Eng Part E: J Process Mech Eng* 235:1587–1597. <https://doi.org/10.1177/09544089211011011>
5. DebRoy T, Wei HL, Zuback JS et al (2018) Additive manufacturing of metallic components – process, structure and properties. *Prog Mater Sci* 92:112–224. <https://doi.org/10.1016/j.pmatsci.2017.10.001>
6. Salmi A, Calignano F, Galati M et al (2018) An integrated design methodology for components produced by laser powder bed fusion (L-PBF) process. *Virtual Phys Prototyp* 13:191–202. <https://doi.org/10.1080/17452759.2018.1442229>
7. Atzeni E, Salmi A (2012) Economics of additive manufacturing for end-use metal parts. *Int J Adv Manuf Technol* 62:1147–1155. <https://doi.org/10.1007/s00170-011-3878-1>
8. Mercelis P, Kruth J-P (2006) Residual stresses in selective laser sintering and selective laser melting. *Rapid Prototyp J* 12(5):254–265
9. Kruth JP, Froyen L, van Vaerenbergh J et al (2004) Selective laser melting of iron-based powder. *J Mater Process Technol* 149:616–622. <https://doi.org/10.1016/j.jmatprotec.2003.11.051>
10. ASM International (2007) *Brazing Handbook*, 5th edn. American Welding Society (AWS)
11. Hedin E (2018) Influence of gap clearance on brazing joint strength for Ni and Fe based filler metals. In: 7th International Brazing and Soldering Conference 2018, New Orleans, Louisiana, USA, pp 155–160
12. Lugscheider E, Humm S (2002) High-temperature brazing of superalloys and stainless steels with novel ductile Ni-Hf-based

- filler metals. *Adv Eng Mater* 4:138. [https://doi.org/10.1002/1527-2648\(200203\)4:3<138:AID-ADEM138>3.0.CO;2-Y](https://doi.org/10.1002/1527-2648(200203)4:3<138:AID-ADEM138>3.0.CO;2-Y)
13. ASM International (2007) Heat treating. In: ASM handbook / prepared under the direction of the ASM International Handbook Committee, vol 4, 10th edn. ASM International, Materials Park, Ohio
 14. Thijs L (2014) Microstructure and texture of metal parts produced by selective laser melting
 15. Chen ZW, Phan MAL, Darvish K (2017) Grain growth during selective laser melting of a Co–Cr–Mo alloy. *J Mater Sci* 52:7415–7427. <https://doi.org/10.1007/s10853-017-0975-z>
 16. Wang SC, Yang Y et al (2016) Investigation of crystal growth mechanism during selective laser melting and mechanical property characterization of 316L stainless steel parts. *Materials & Design* 100:291–299. <https://doi.org/10.1016/j.matdes.2016.03.111>
 17. Sun Z, Tan X, Tor SB et al (2016) Selective laser melting of stainless steel 316L with low porosity and high build rates. *Materials & Design* 104:197–204. <https://doi.org/10.1016/j.matdes.2016.05.035>
 18. Saeidi K, Gao X, Lofaj F et al (2015) Transformation of austenite to duplex austenite-ferrite assembly in annealed stainless steel 316L consolidated by laser melting. *J Alloys Compd* 633:463–469. <https://doi.org/10.1016/j.jallcom.2015.01.249>
 19. Saeidi K, Gao X, Zhong Y et al (2015) Hardened austenite steel with columnar sub-grain structure formed by laser melting. *Mater Sci Eng A* 625:221–229. <https://doi.org/10.1016/j.msea.2014.12.018>
 20. VDI VDI 3405:2014-12 Additive manufacturing processes, rapid manufacturing - basics, definitions, processes. VDI 3405
 21. Sekulić DP (2013) Advances in brazing: science, technology and applications. In: Woodhead publishing in materials. Woodhead Publishing, Cambridge, UK, Philadelphia, PA
 22. Reinkensmeier I, Blank R, Hermann O (2019) Reinkensmeier et al. - Löten SLM-gefertigter Turbinen-Komponenten des Heißgasbereichs aus Nickellegierungen. *Schweißen und Schneiden*:214–220
 23. Xia C, Zhao M, Sun W et al (2019) Microstructure and properties of 3D printed Inconel 718 joint brazed with BNi-2 amorphous filler metal. *Mat Res* 22:791. <https://doi.org/10.1590/1980-5373-mr-2018-0348>
 24. Tillmann W, Henning T, Wojarski L (2018) Vacuum brazing of 316L stainless steel based on additively manufactured and conventional material grades. *IOP Conf Ser: Mater Sci Eng* 373:12023. <https://doi.org/10.1088/1757-899X/373/1/012023>
 25. Tillmann W, Wojarski L, Henning T (2021) Investigation of joints from laser powder fusion processed and conventional material grades of 18MAR300 nickel maraging steel. *Weld World* 65:1323–1331. <https://doi.org/10.1007/s40194-021-01096-1>
 26. Krakhmalev P, Yadroitsava I, Fredriksson G et al (2017) Microstructural and thermal stability of selective laser melted 316L stainless steel single tracks. *SAJIE* 28. <https://doi.org/10.7166/28-1-1466>
 27. Ronneberg T, Davies CM, Hooper PA (2020) Revealing relationships between porosity, microstructure and mechanical properties of laser powder bed fusion 316L stainless steel through heat treatment. *Mater Des* 189:108481
 28. Li Y, Shen Y, Zhong S et al (2021) Investigation on properties of joints vacuum brazed with nickel-based adhesive tape filler metal. In: 3rd International Conference on Artificial Intelligence and Advanced Manufacture. ACM, New York, NY, USA, pp 2594–2598
 29. Penyaz MA, Ivannikov AA, Sevryukov ON et al (2021) Overview of nickel-based filler metals for brazing of austenitic stainless steels. *Chin J Nonferrous Met* 1:41–56. <https://doi.org/10.17580/nfm.2021.01.06>
 30. Zhang M, Sun C-N, Zhang X et al (2018) Effect of heat treatment on fatigue crack initiation of laser powder bed fusion stainless steel 316L. *Matec Web Conf* 165:22006. <https://doi.org/10.1051/mateconf/201816522006>
 31. Korinko PS, Morgan MJ Effect of heat treatment on the properties of additively manufactured type 316L stainless steel. In: Pressure vessels and piping conference. American Society of Mechanical Engineers
 32. Diepold B, Neumeier S, Meermeier A et al (2021) Temperature-dependent dynamic strain aging in selective laser melted 316L. *Adv Eng Mater* 23:2001501. <https://doi.org/10.1002/adem.202001501>
 33. Salman OO, Gammer C, Chaubey AK et al (2019) Effect of heat treatment on microstructure and mechanical properties of 316L steel synthesized by selective laser melting. *Mater Sci Eng A* 748:205–212. <https://doi.org/10.1016/j.msea.2019.01.110>
 34. Park J-M, Kim S-H, Jeong M-H et al (2014) Effect of Cu–Sn intermetallic compound reactions on the Kirkendall void growth characteristics in Cu/Sn/Cu microbumps. *Jpn J Appl Phys* 53:05HA06. <https://doi.org/10.7567/JJAP.53.05HA06>
 35. Leone EA, Rabinkin A, Sarna B (2006) Microstructure of thin-gauge austenitic and ferritic stainless steel joints brazed using Metglas® amorphous foil. *Weld World* 50:3–15. <https://doi.org/10.1007/BF03266509>
 36. Ivannikov AA, Penyaz MA, Dzhumaev PS et al (2021) Diffusion brazing of stainless steels influence of Ni-B filler alloy composition. *Weld World* 65:317–328. <https://doi.org/10.1007/s40194-020-01013-y>
 37. Rabinkin A, Wenski E, Ribaldo A (1998) Brazing stainless steel using a brazing stainless steel using a new MBF-series of Ni–Cr–B–Si amorphous brazing foils. *Weld J* 77:66–75

Publisher's note Springer Nature remains neutral with regard to jurisdictional claims in published maps and institutional affiliations.